Micromixer based on viscoelastic flow instability at low Reynolds number

Micromixer based on viscoelastic flow instability at low Reynolds number

Y.C. Lam, H.Y. Gan and N.T. Nguyen

Abstract

We exploited the viscoelasticity of biocompatible dilute polymeric solutions, namely dilute poly (ethylene oxide) solutions, to significantly enhance mixing in microfluidic devices at very small Reynolds number, i.e. Re ≈ 0.023, but large Peclet and Elasticity numbers. With an abrupt contraction micro-geometry (8:1 contraction ratio), two different dilute poly (ethylene oxide) solutions were successfully mixed with a short flow length at a relatively fast flow velocity. Micro-particle image velocimetry (μPIV) and fluorescent concentration measurements were employed in our investigations to characterize the flow fields and mixing efficiency. The results showed that enhanced mixing can be achieved through viscoelastic flow instability under situations where molecular diffusion and inertia effects are negligible. This approach bypasses the laminar flow limitation, usually associated with low Reynolds number, which is not conducive to mixing.

Keywords: Viscoelastic, Microchannel, Mixing, Flow instability

Yee Cheong Lam, Professor

School of Mechanical & Aerospace Engineering, Division of Manufacturing Engineering,

Nanyang Technological University, 50 Nanyang Avenue, Singapore 639798.

Corresponding author. E-mail: myclam@ntu.edu.sg; Fax: 65 6791 1895; Tel: 65 6790 5866

Hiong Yap Gan, Mr.

School of Mechanical & Aerospace Engineering, Division of Manufacturing Engineering,

Nanyang Technological University, 50 Nanyang Avenue, Singapore 639798.

Nam-Trung Nguyen, Associate Professor

School of Mechanical & Aerospace Engineering, Division of Thermal and Fluids Engineering,

Nanyang Technological University, 50 Nanyang Avenue, Singapore 639798.

Acknowledgment

The authors would like to thank the Agency of Science, Technology and Research, Singapore (A*Star) for its financial support (SERC grant no. 052 101 0013). The second author gratefully acknowledges the supports provided by A*Star in the form of an A*Star Graduate Scholarship and other supports received from its affiliated institution, the Singapore Institute of Manufacturing Technology (SIMTech). PEO powder was provided by The Dow Chemical Company. This research is protected by a US provisional patent application no. 67/701,078.

1. Introduction

A key attribute of flow dynamic in microdevices is their laminar character, which is in sharp contrast to the easily achievable turbulent flow in macroscopic process equipment. As a result, mixing fluids in microchannels is challenging and often an obstacle to achieve good performance in microfluidics systems (Ottino and Wiggins, 2004). The reason for predominantly laminar flow in microdevices is their microscale dimensions, which lead to a small Reynolds number

$$\mathrm{Re} = \rho \bar{V} d_o / \eta_o \qquad (1)$$

where ρ, $\bar{V}$, d_o, and η_o are the fluid density, the average velocity, the characteristic length, and the viscosity respectively. Viscous effects become dominant in microscale and suppress viscous-inertial flow instabilities. Consequently, mixing of multiple streams in microchannels often relies on molecular-diffusion mechanism, and not on the effective mechanism of chaotic/turbulent flow instability (Stone *et al.*, 2004; Nguyen and Wu, 2005). In general, miromixers can be categorized as passive micromixers and active micromixers (Nguyen and Wu, 2005). Passive micromixers, which include lamination and chaotic advection micro-mixers, rely on the diffusive mixing mechanism. They require long and complicated channel geometry. Although active micromixers might be employed, they require external actuators. Both methods lead to complex and expensive fabrication processes. A different approach that bypasses the limitation of the low Reynolds number, yet provides efficient mixing, will be a significant improvement for microfluidic system design.

Solutions with trace amount of highly deformable polymers are viscoelastic fluids. These fluids, which are non-Newtonian, have a complex internal microstructure which can lead to counterintuitive flow and stress responses. The stress experienced by these fluids will not immediately become zero with the cessation of driving force and fluid motion, but decaying with a characteristic time due to its elasticity. By employing these fluids, viscoelastic flow instability can be generated in microfluidic device at very low Re (Re < 1). Burghelea *et al.* (2004) had recently extended the works of Groisman and Steinberg (2001) for viscoelastic mixing in millimeter length scale to micrometer length scales. Chaotic flow instabilities were exploited for enhancement of mixing at very low Reynolds numbers. Efficient mixing was demonstrated with a relatively long mixing channel at a moderate flowrate. The characteristic mixing times of these viscoelastic fluids were reduced by 3 to 4 orders of magnitude as compared to mixing based on the mechanism of molecular diffusion.

Indeed, to exploit effectively the viscoelasticity of fluids for chaotic flow instability, and thus mixing, sharper and smaller geometries should be employed (Bird *et al.*, 1987). Stress singularities developed at such corners have been the source of elastic instabilities in many macro-scale experiments for fluids with viscosity in at least O(Pa·s), while rounded corners tend to suppress elastic behavior (Evans and Walter, 1986; Evans and Walter, 1989). The distinct similarities of these nonlinear flow phenomena at micro-length scale experiments were demonstrated qualitatively in a microdevices with dilute viscoelastic fluids, with viscosity in O(mPa·s). For instance, in converging entry flow via a planar contraction micro-geometry at a relatively low Reynolds number (Re < 10) (Rodd *et al*. (2005)) and for flow in a flip-flop memory devices (Groisman *et al.*, 2003). The elastic effects were demonstrated to be dominant and they induced flow instability in an abrupt convergent/divergent micro-length scale flow system.

The promotion of viscoelastic instability by utilizing microchannels with abrupt contraction/expansion geometry for micromixing was recently exploited by Gan *et al.* (2006a, 2006b). Their mixing experiments have very high values of Elasticity numbers (a ratio of elastic to inertial forces of the system), which are approximately 932 and 5070. At such a high Elasticity number, inertial effects were negligible. Thus, Reynolds number (a ratio of inertial to viscous forces of the system) is no longer relevant in describing the flow behaviors. The flow dynamics, and thus mixing, of two dissimilar viscoelastic fluid streams were mainly governed by the competition of the viscous and elastic forces in the flow field. As such, Deborah number, which is a ratio of elastic to viscous forces of the system, would be the dominant governing parameter.

In the current investigation, we analyze the flow dynamics of mixing two dissimilar viscoelastic fluids through a converging/diverging flow system based on the measurements of both velocity flow field and fluorescence concentration field. Dilute poly-ethylene oxide (PEO) fluids were employed for its inherent viscoelastic effects and its biocompatibility such that any residual should not induce inflammatory response. In addition, PEO is water-soluble, avoiding the usage of potentially toxic organic solvents for dissolving it (Washburn *et al.*, 2002).

2. Materials and Methods

2.1 Device fabrication and setup

We employed a microchannel with a depth of 150 μm and an abrupt contraction/expansion of 1000:125:1000 μm to introduce the convergent/divergent flow. The length of the contraction was 1000 μm. Side streams were introduced into the central main stream through two side channels, each at either side of the main channel. The side channels are 1000 μm in width and located 3000 μm upstream from the centerline of the contraction. The channel structures were realized in a silicon/glass chip, see Figure 1. The microchip was made by silicon wafer and Pyrex glass wafer. A polymeric holder was designed and fabricated as the micro/macro fluidic interface. Details on device fabrication are contained in Gan *et al.* (2006b).

The sample fluids were delivered by a precision syringe pump (Lomir Biomedical Inc.). The mainstream flowrate was $0.5\dot{Q}$, with both side streams having the same flowrate of $0.25\dot{Q}$. Thus, the total flow rate was $\dot{Q}$. This flow rate ratio was achieved by driving simultaneously three different syringes with the appropriate size ratio by the same pump. The total volumetric flow rates used in the experiments were 0.5, 5 and 10 ml/h.

2.2 Fluid preparations

The mainstream fluid consists of 1 wt% PEO in 55 wt% glycerol water and green fluorescent dye. For brevity, this fluid is denoted as 1% PGW. The fluid of the side streams consists of 0.1 wt% PEO in water, and 3-μm red fluorescent microspheres. For brevity, this fluid is denoted as 0.1% PW. The mainstream fluid (1% PGW) has a higher viscosity and elasticity than the side streams fluid (0.1% PW), see Table 1. The mean molecular weight (M_w) of PEO (supplied by The Dow Chemical Company) is approximately 2×10^6 g/mol. For fluorescence concentration measurements, a fluorescent dye (fluorescein disodium salt $C_{20}H_{10}Na_2O_5$) was added to 1%PGW at a weight ratio of 3×10^{-4}:1. A solution of dispersed 3-μm red fluorescent microsphere (6.7×10^{11} Number/mL, Duke Scientific Co.) was added to 0.1% PW at a volume ratio of 0.1:1. These fluorescent microspheres serve as tracing particles in the μPIV measurements.

2.3 Rheological property measurements

Table 1 lists the rheological properties of the fluid. All the fluid properties were determined with the additives. Relaxation times (λ) were computed from the ratio of storage modulus (G') and loss modulus (G"). The values of G' and G" were determined under shear stress in a frequency oscillation test (Rheometrics Scientific, - ARES - Advanced Rheometric Expansion). The steady shear viscosities were determined using a strain controlled – steady rate sweep test with shear rates in the range of $0.1 \leq \dot{\gamma} \leq 100$ s^{-1}. Due to the dilute viscosity of 0.1%PW, its λ could not be determined with our facility and its value was taken from Rodd *et al*. (2005). The viscosity of 0.1%PW was determined using the viscometer Contraves LS 40 (controlled rate mode). The diffusion coefficient of the dye in water was $D = 1.5\times10^{-9}$ m^2/s (Wu *et al.*, 2004). Since diffusion coefficient is inversely proportional to the viscosity (Einstein, 1956), we estimated that $D = 1.47\times10^{-12}$ m^2/s for 1% PGW, indicating that mixing based on diffusion mechanism is negligible.

2.4 Dimensionless Parameters

For mixing in laminar flow, diffusion is an important mechanism. Peclet number, Pe, indicates the relative importance of advection to diffusion, and is given by

$$\mathrm{Pe} = \dot{Q}L_{\mathrm{char}} / D(w_c d) \qquad (1)$$

where L_{char} is the upstream channel width, D is the diffusion coefficient and $\dot{Q}$ is the total volumetric flow rate. The higher the Pe, the less significant is diffusion.

For an aqueous or a viscous solution, the onset of flow instability can be characterized by the Reynolds number, Re, which measures the relative importance of inertial and viscous effects in a fluid flow. It can be defined as

$$\mathrm{Re} = 2\rho\dot{Q} / \eta_o(w_c + d) \qquad (2)$$

where d is the channel depth, w_c is the contraction width. ρ and η_o are the fluid density and viscosity, respectively.

For a given geometry, the viscoelastic effects of a fluid flow can be characterized by the Deborah Number, De. The Deborah number is a dimensionless parameter which typifies the relative importance of the elastic stresses of the fluid with the time scale of the flow system (Bird

et al., 1987). Generally, smaller dimension results in a higher characteristic deformation rate for the same flow rate, resulting in higher elastic effects and a higher De.

Deborah number can be expressed based on the characteristic shear rate,

$$\mathrm{De} = \lambda \dot{\gamma}_{char} = \lambda(2\dot{Q}/w_c^2 d) = 2\lambda\dot{Q}/w_c^2 d \quad (3)$$

The characteristic shear rate is $\dot{\gamma}_{char} = \overline{v}_c/(w_c/2) = (\dot{Q}/w_c d)/(w_c/2) = 2\dot{Q}/w_c^2 d$, λ is the relaxation time of the viscoelastic fluid measured in shear and $\overline{v}_c$ is the average flow velocity.

A smaller channel has smaller flow characteristic length and time. Thus, Re is smaller and it is difficult to have inertia/viscous flow instability. Conversely, De becomes larger and it is easier to have elastic/viscous instability. The relative dominance of elastic to inertial effects is typified by the elasticity number, El, i.e. the ratio of fluid elasticity to fluid inertia. El is expressed as

$$\mathrm{El} = \mathrm{De}/\mathrm{Re} = \frac{2\lambda\eta_0(w_c + d)}{\rho w_c^2 d} \quad (4)$$

El is a function of the given fluid and geometry. It is dependent on the fluid properties and the inverse of the characteristic cross-sectional area.

With reference to the mainstream fluid (1% PGW) properties, experiments are performed over a range of De and Re ($21.73 < \mathrm{De} < 434.6$, $0.001 < \mathrm{Re} < 0.023$). The elasticity number ($\mathrm{El} = 19.3 \times 10^3$) is constant for a given fluid and geometry and is dependent only on the fluid properties and the inverse of the characteristic cross-sectional area. With this enormous elasticity number, this flow regime has negligible inertial effects and can be characterized by De alone. The Peclet number (Pe) for all viscoelastic fluid flow experiments were large ($\mathrm{Pe} > 5.04 \times 10^6$). Thus, mixing based on molecular diffusion is negligible.

2.5 Imaging techniques

The experimental setup, for both measurements of the velocity and the concentration fields is depicted schematically in Figure 2. Basically, the setup consists of four main components: an illumination system, an optical system, image acquisition devices and a control system. Two different illumination sources, a double pulsed Q-switch (quality switched) Nd:YAG laser and a mercury lamp, were used for the measurements of the velocity field and the concentration field. The optical system consisted of an inverted microscope (Model ECLISPE TE2000-S) with a set of epi-fluorescent attachments. The image acquisition

devices consists of an interline transfer CCD camera (HiSense MkII), a FlowMap system hub with last-in-first-out (LIFO) capability and a commercial camcorder (Sony, DCR-DVD803E). The resolution of the CCD camera is 1344×1024 pixels with 12 bits grayscale. The recorded images were digitally transferred to a personal computer for further analysis.

For each flowrate, the flow field images in the same experiment were visualized using the green fluorescent dye (main stream) and the red fluorescent microspheres (side streams). The images of the streams, at the same area of interest, were captured by switching the epi-fluorescent attachments of the microscope. The green fluorescent dye has an excitation wavelength and an emission wavelength of 490 and 520 nm, respectively. The epi-fluorescent attachment of type Nikon B-2A (excitation filter for 450–490 nm, dichroic mirror for 505 nm and an emission filter for 520 nm) was used for the green dye. The red microspheres (Duke Scientific Co.) with an excitation wavelength of 540 nm and a maximum emission wavelength of 610 nm were imaged with the epi-fluorescent attachment of type Nikon G-2E/C (excitation filter for 540 nm, dichroic mirror for 565 nm and an emission filter for 605 nm). The relatively large red microspheres help to minimize the diffusive effect in the experiments. Both green and red filters have a bandwidth of 25 nm.

3. Results and Discussions

3.1 Measurement of the velocity field

As fluorescent microspheres were added only to the side streams (0.1% PW) for μPIV investigations, only the flow field of the side streams would be measured. The microspheres have a maximum excitation wavelength close to the characteristic wavelength of Nd:YAG laser. The measurement was carried out with a 4× objective lens and two 30 mJ laser pulses with a delay time of 4 ms. At least 50 images were collected for every flow condition. The fluorescent microspheres solution was not added to the higher viscosity 1% PGW. This would ensure that any velocity measured was related to particles originated from the side streams. This would allow us to evaluate easily the penetration of the side streams to the main stream. In addition, if the solution was added to the main stream, it would compromise the viscosity of the main stream due to the exponential relationship of viscosity to the concentration of the polymeric solution, particularly the solvent glycerol.

Figure 3 shows the typical results obtained from the μPIV measurement upstream of the contraction. For viscoelastic two-fluid flow at $\dot{Q}$= 10 ml/h, asymmetrical vortices was

observed and confirmed with post-analysis (streamlines and velocity vector field) using a commercial PIV software (Flow Manager, FlowMap). The formation of these asymmetrical vortices based on empirical observations was discussed in our previous work (Gan *et al.*, 2006a; 2006b).

Figure 4 presents the consecutive velocity fields of viscoelastic two-fluid flow at $\dot{Q}$= 10 ml/h. Salient and large corner vortices with viscoelastic "whipping" at upstream of the contraction were evident. Successive snapshots show a large fluctuation of both magnitude and direction of the velocity vectors. This fluctuation indicates the highly instable nature of the viscoelastic flow. The results illustrated the chaotic competition of the two fluids at the contraction and across the downstream channel. These results were in good agreement with our earlier observations. Significant mixing of the two viscoelastic fluids was expected and observed.

Figures 5 to 7 show the statistical analyses of the velocity flow profile for three different flowrates, 0.5, 5 and 10 ml/h, respectively. At $\dot{Q}$= 0.5 ml/h, the entire flow field was stable and steady. The flow was laminar and the measured results show a small variance in velocity, see Figure 5. For the upstream velocity profile shown in Figure 5(a), no data points were shown at the central portion due to the lack of fluorescent microspheres in the mainstream. The downstream velocity profile (Figure 5(b)) shows large variances at the central portion of the channel. This phenomenon was caused by the penetration of fluorescent microspheres from the side streams into the mainstream. This penetration was intermittent but consistent. However, in general, the entire flow field shows little flow instability.

At higher flow rates, i.e. $\dot{Q}$= 5 ml/h, salient corner vortices were formed upstream of the contraction. For $\dot{Q}$= 5 ml/h, the upstream vortices were larger than in $\dot{Q}$= 0.5 ml/h but remained rather constant in size. The entire flow field was still rather laminar-like. This fact was supported by the symmetrical velocity profile plot with an increasing, but still relatively small variance, see Figure 6. As shown in Figure 6(a), at upstream of the contraction, there was a region at the center portion of the channel with much higher velocity. This indicated the side streams particles had penetrated into the mainstream and their velocity increased due to the transfer of momentum from the mainstream to these side stream particles. As shown in Figure 6(b), at downstream of the contraction, one can observe more penetrations

of the side streams into the central portion of the channel, with increasing fluctuation of the flow field at the center portion of the channel.

At the highest flowrate investigated, i.e. $\dot{Q}$= 10 ml/h, the upstream vortices were the largest and unstable in nature. “Elastic whipping” of the central mainstream was observed upstream of the contraction, with inter-penetration of mainstream and side streams. As shown in Figure 7(a), the results show a competition between the main and the side streams at the entrance of the contraction with significant velocity fluctuation. The entire flow field became unstable and chaotic. The whipping effects allowed the side streams to penetrate deeply into the central portion downstream, see figure 7(b). Extensive flow stability occurred downstream of the contraction as indicated by the large velocity variance. Indeed, the well defined parabolic average velocity profile (solid line) in figure 7(a) was much less obvious in figure 7(b), suggesting the possibility of the onset of turbulent flow. In addition, with deep penetration of the side streams into the main stream, and with flow instability, it is expected that effective mixing would result in the microchannel.

3.2 Measurement of concentration field

Concentration measurements were conducted in order to evaluate the efficiency of mixing for the highest flowrate investigated, namely $\dot{Q}$= 10 ml/h. The measured area was illuminated by a mercury lamp. The mainstream with green fluorescent dye (Figures 8(a) & (c)) was employed as the reference for evaluating the mixing performance. The side streams with red microspheres, which appeared as red streak flow (Figures 8(b) & (d)) would track the flow of the side streams. After recording the CCD images on a PC (Figure 9(a) & (b)), the concentration profiles were evaluated using a customized program written in MATLAB. The noise in the measured image was removed with an adaptive noise-removal filter. For each pixel, a local mean value is calculated with a window of 5×5 pixels. The noise distribution is assumed to have a Gaussian characteristic.

For benchmarking, de-ionized water (DI water), which is a Newtonian liquid with negligible elasticity and low viscosity, was first investigated, see Figures 8(a)-(b). Thus, viscous-inertial effects dominated the entire flow field. At upstream of the contraction, the interface between the streams was well defined and stable. A pair of symmetrical corner vortices (lip vortices) were formed immediately downstream of the contraction due to the expansion flow effects and is in good agreement with previously reported results (Drikakis, 1997; Hawa and

Rusak, 2001). There were some spreads of the main stream at downstream of the contraction possibly due to the sudden expansion flow immediately after the contraction. However, no penetration of the side streams into the main stream was observed.

The concentration measurements for the viscoelastic fluids (1% PGW and 0.1% PW) were shown in Figures 8(c)-(d). At upstream of the contraction, salient and large corner vortices with repeated whipping of the mainstream across the channel width previously observed in velocity measurements (figure 3) could also be observed here, see Figures 8(c)-(d). Mixing was expected as there was overlapping region of the green fluorescent dye (main stream) and red microspheres (side streams). Indeed, it was observed that the main stream also penetrate into the two side vortices of the side streams. At downstream of the contraction, due to the more pronounced viscoelastic flow instability as described previously, other than a thin layer next to the edge of the channel wall, significant mixing had occurred over the entire channel cross section, see Figures 8(c)-(d). The observed mixing regions were consistent with the viscoelastic instability regions and phenomena observed through the measurements of the velocity field as described in the previous section.

Mixing performance of the mean flow was evaluated from the probability density function (PDF) of the intensity images, i.e. concentration measurements. The intensity of the grayscale in the recorded images is proportional to the green dye concentration. Details on quantifying mixing efficiency, ε_{eff}, from the PDF of intensity images are contained in Gan *et al.* (2006b). The mixing efficiency ε_{eff} is quantified based on the following definition,

$$\varepsilon_{eff} = \left[1 - \frac{\sum_{C_i=0}^{C_i=1} |C_i - C_\infty| P(C_i)}{C_\infty} \right] \times 100\% \qquad (5)$$

where C_i is the observed concentration on the normalized scale, C_∞ is the concentration on the normalized scale for perfect mixing, and $P(C_i)$ is the probability density function. In our investigation, for equal flow rate of the main and the side streams, perfect mixing concentration is C_∞= 0.5. With eq.(5), ε_{eff} = 0% for no mixing and ε_{eff} = 100% for perfect mixing.

Figure 9 compares the progression of ε_{eff} along the flow path for the Newtonian fluids (DI water) and the viscoelastic fluids at the same total flow rate of $\dot{Q}$= 10 ml/h. It was demonstrated by evaluating the ε_{eff} across the channel at various locations along the flow path for both upstream and downstream channels. The size of analysis window is an area of 30 μm x 950 μm across the channel. The analysis windows were distributed evenly at a spacing of 100 μm except at the proximity of the contraction plane, where the spacing interval is halved, see Figure 9 (a) & (b).

Figure 9(c) shows the progression of ε_{eff}. At upstream of contraction, for the laminar flow of DI water, there was insignificant mixing (approximately 12% on average). For the viscoelastic fluids flow, on average more than 15% of mixing was found along the upstream channel. Maximum mixing of 30% were observed at a distance of 1.2 mm approximately (section 11 upstream) away from the contraction plane. Indeed, one would expect that ε_{eff} could only increase as flow progressed. Thus, it was interesting to observed that as flow progressed from sections 11 to 1 upstream, ε_{eff} decreased. The surge of ε_{eff} at section 11 was due to the relatively large fluctuation in the flow field or viscoelastic whipping as compared to the region near to the contraction. The scale of whipping was constrained by the converging flow path when approaching the contraction plane. In addition, close to the contraction, the mainstream, and fluids next to the mainstream, which consisted of a mixture of mainstream and sidestreams, were "compressed" and flow at a higher velocity. As such, more of the unmixed side streams would dominate spatially resulting in lower mixing efficiency ε_{eff}.

At downstream of contraction, mixing performance for the DI water flow had improved due to the expansion flow effects. Mixing region at the interface of the two streams was stretched out. $\dot{\varepsilon}_{eff}$ had improved from 10% to 30%. Highly concentrated main and side streams could still be identified easily from the CCD images, see figure 9(a). This low efficiency of mixing was as expect for Newtonian flow at this low Reynolds number (Re ≈ 20.2) and large Peclet number (Pe ≈ 98.8×10^3).

For viscoelastic fluids flow downstream of the contraction, viscoelastic flow instability together with the expansion flow effects had promoted mixing effectively. Next to the

contraction, ε_{eff} was approximately 50%. This was mainly caused by the inhomogeneous volume of fluids discharged through the contraction intermittently, due to the frantic competition of the two streams at upstream of the contraction. As flow progressed further downstream, mixing was further promoted through viscoelastically induced flow instability, and $\dot{\varepsilon}_{eff}$ increased steadily from 50% to 70%, see Figure 9(c). Indeed, the CCD image in Figure 9((b) shown extensive overlapping of the two fluids. Thus, despite of the very low Reynolds number ($\mathrm{Re} \approx 0.023$) and a large Peclet number ($\mathrm{Pe} \approx 101 \times 10^6$), significant mixing was achieved.

4. Conclusions

Viscoelastic flow instability was achieved by employing viscoelastic fluids with simple convergent-divergent channel geometry. The proposed device was simple yet effective for mixing over a short distance, and at a relatively high flowrate. This flow regime has a negligibly small Reynolds number but very high Deborah number and Peclet number. This mixing approach bypasses the limitation of low Reynolds number in microfluidic applications. This micromixer can potentially be implemented in a lab-on-a-chip platform with minimum requirements for design and fabrication. However, further improvement is required to minimize the pressure drop in achieving a fast flow rate to elastically induce flow instability.

Table 1. Fluid properties [a]

Fluid	Zero-shear viscosity η_o (Pa .s)	Density ρ (kg/m^3)	Relaxation time λ (s)
0.1% PW with micro-spheres	2.24×10^{-3}	0.997×10^3	1.5×10^{-3}
1% PGW with fluorescence dye	1020×10^{-3}	1.13×10^3	220×10^{-3}

[a] Measurement recorded at 25 ± 1 °C

References

R.B. Bird, R.C. Armstrong and O. Hassager, Dynamics of Polymeric Liquids. 1, (John Wiley & Sons, New York, 1987).

T. Burghelea, E. Segre, I. Bar-Joseph, A. Groisman and V. Steinberg, Phys. Rev. E 69, 066305 (2004).

D. Drikakis, Phys. Fluids 9, 76 (1997).

A. Einstein, Investigation on the Theory of the Brownian Movement (Dover, 1956).

R.E. Evans and K. Walter, J. Non-Newt. Fluid Mech. 20, 11 (1986).

R.E. Evans and K. Walter, J. Non-Newt. Fluid Mech. 32, 95 (1989).

H.Y. Gan, Y.C. Lam and N-T. Nguyen, App. Phys. Lett. 88, 224103 (2006a).

H.Y. Gan, Y.C. Lam, N-T. Nguyen, K.C. Tam and C. Yang, Microfluidics and Nanofluidics xx, xx (2006b). (in press)

A. Groisman, M. Enzelberger and S.R. Quake, Science 300, 955 (2003).

A, Groisman and V. Steinberg, Nature 410, 905 (2001).

T. Hawa and Z. Rusak, J. Fluid Mech. 436, 283 (2001).

N-T. Nguyen and Z. Wu, J. Micromech. Microeng. 15, R1 (2005).

J.M. Ottino and S. Wiggins, Science 305, 485 (2004).

L.E. Rodd, T.P. Scott, D.V. Boger, J.J. Cooper-White and G.H. McKinley, J. Non-Newt. Fluid Mech. 129, 1 (2005).

H.A. Stone, A.D. Stroock and A. Ajdari, Annu. Rev. Fluid Mech. 36, 381 (2004).

N.R.Washburn, C.G. Simon Jr, A. Tona, H.M. Elgendy, A. Karim and E.J.Amis, J Biomed Mater Res. 60, 20 (2002).

Z. Wu, N-T. Nguyen and X. Huang, J. Micromech. Microeng. 14, 604 (2004).

List of figure caption

Figure 1. Silicon-glass micromixer: (a) Silicon-glass micromixer and the polymeric holder, (b) Geometry of the microchannel, and (c) The assembled micromixer. (Adapted from Gan *et al.* 2006b)

Figure 2. Optical setup for fluorescent concentration and PIV measurements.

Figure 3. Typical results of two-dissimilar viscoelastic fluid flow ($\dot{Q}$ = 10 ml/h, trace microspheres are in the side streams): (a) raw particle image, (b) evaluated streamlines of the flow field, (c) evaluated velocity field, and (d) surface plot of the velocity magnitude

Figure 4. Consecutive PIV measurements for viscoelastic fluids flow ($\dot{Q}$ = 10 ml/h, trace microspheres are in the side streams): (a) t = 0 s (arbitrary), (b) t = 2.4 s, and (c) t = 4.8 s.

Figure 5. Velocity profile across the channel at $\dot{Q}$ = 0.5 ml/h (each plot represents statistic over 50 image pairs and 1,000 data points): (a) upstream of the contraction and (b) downstream of the contraction.

Figure 6. Velocity profile across the channel at $\dot{Q}$ = 5 ml/h (each plot represents statistic over 50 image pairs and 1,000 data points): (a) upstream of the contraction and (b) downstream of the contraction

Figure 7. Velocity profile across the channel at $\dot{Q}$ = 10 ml/h (each plot represents statistic over 50 image pairs and 1,000 data points): (a) upstream of the contraction and (b) downstream of the contraction.

Figure 8. Images from concentration measurements of water (a-b) and viscoelastic fluids (c-d) in microchannels with 8:1 contraction ratio at $\dot{Q}$ = 10 ml/h. (a) - (b): Laminar and stable flow for both upstream and downstream. Due to inertial/viscous effects, vortices were formed at the corners downstream of contraction, resulting in insignificant mixing downstream. (c) – (d): Significant and extensive mixing indicated by extensive overlapping of the fluorescent dye and microspheres. Upstream of the contraction, viscoelastic whipping of main stream and large salient corner vortices induced primarily by side streams. Downstream of contraction, expansion flow of the main stream, and chaotic flow. Both flow expansion and chaotic flow contributed effectively to mixing. Mixing extended across the entire cross section, except for thin boundary layers next to channel walls.

Figure 9. Progressing of mixing along the flow path for both DI water and viscoelastic fluids at upstream and downstream channels. (a) & (b) -- Rectangular box represents the analysed window for the evaluation of mixing efficiency at a specific location. (c) Progression of mixing performance along the flow path at $\dot{Q}$ = 10 ml/h.

Figure1

Click here to download high resolution image

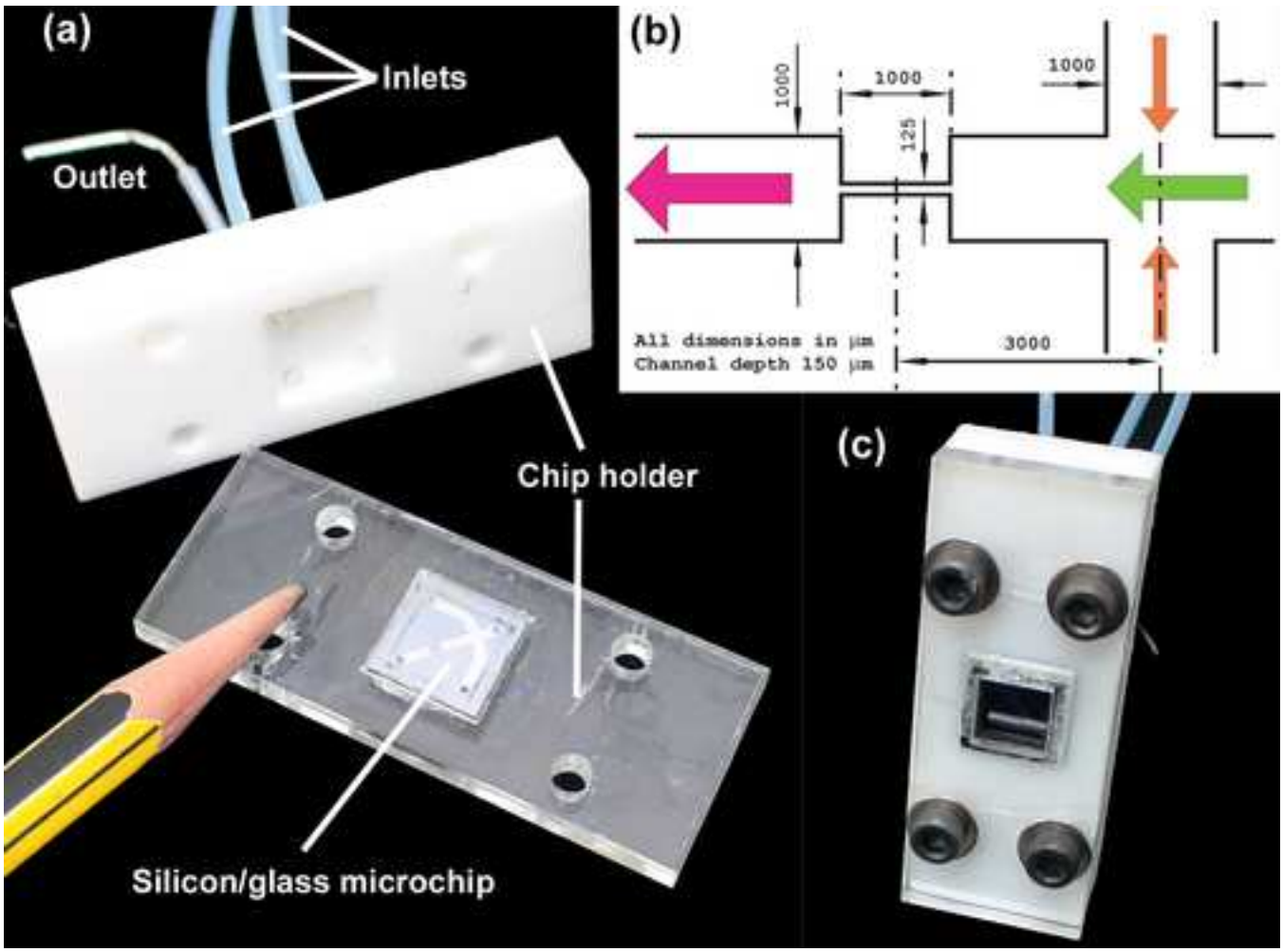

Figure2

Click here to download high resolution image

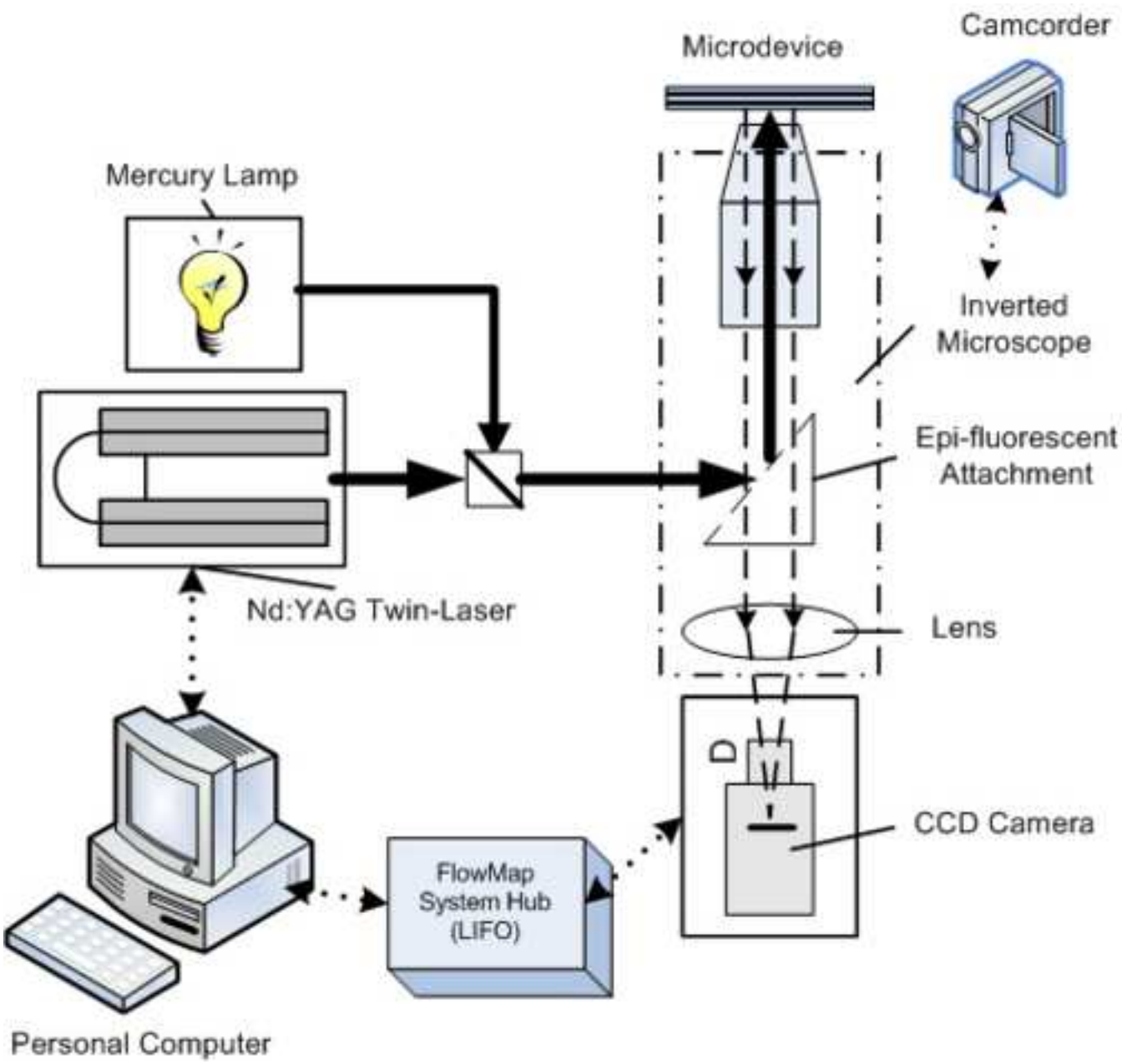

Figure3

Click here to download high resolution image

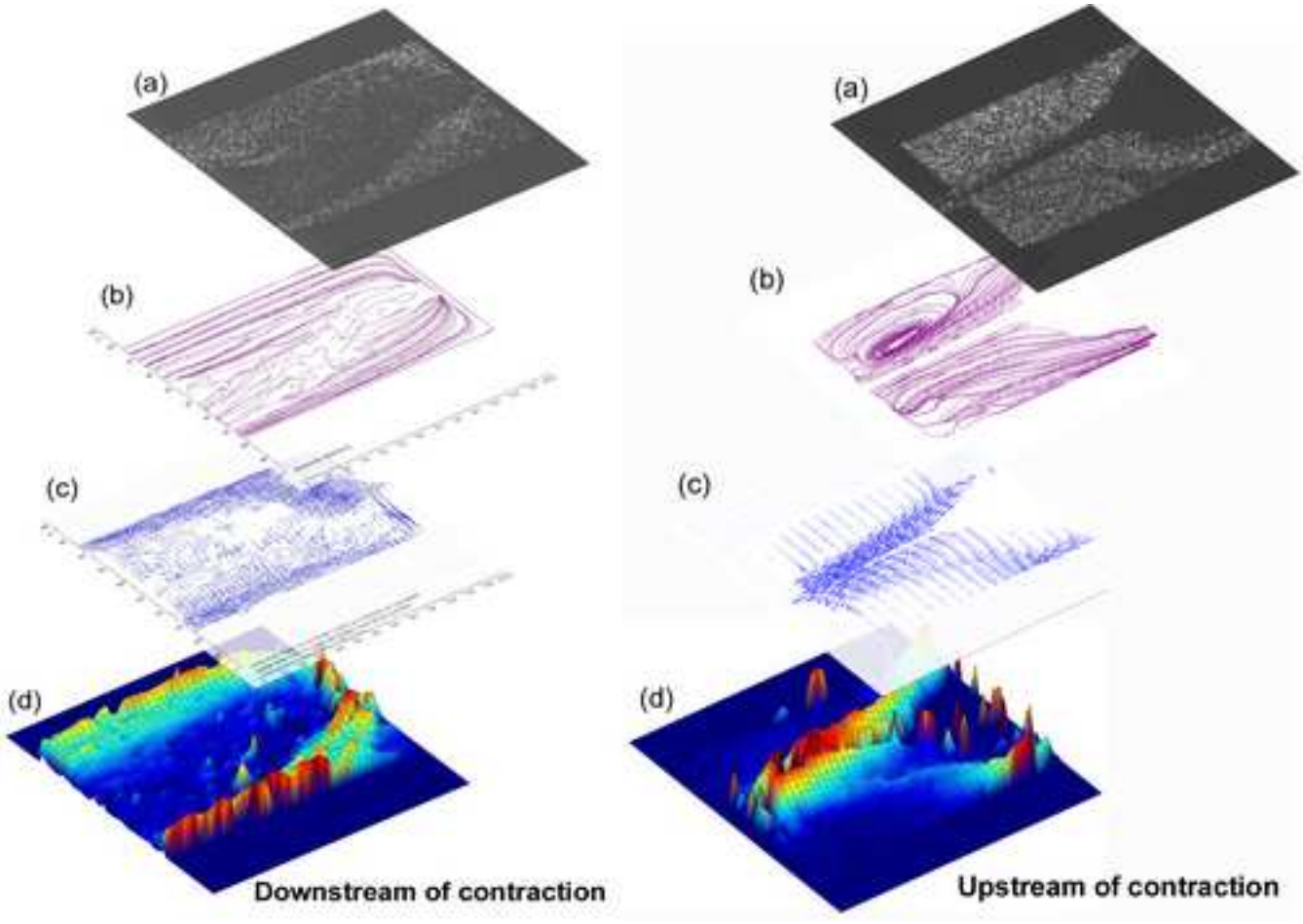

Figure4

Click here to download high resolution image

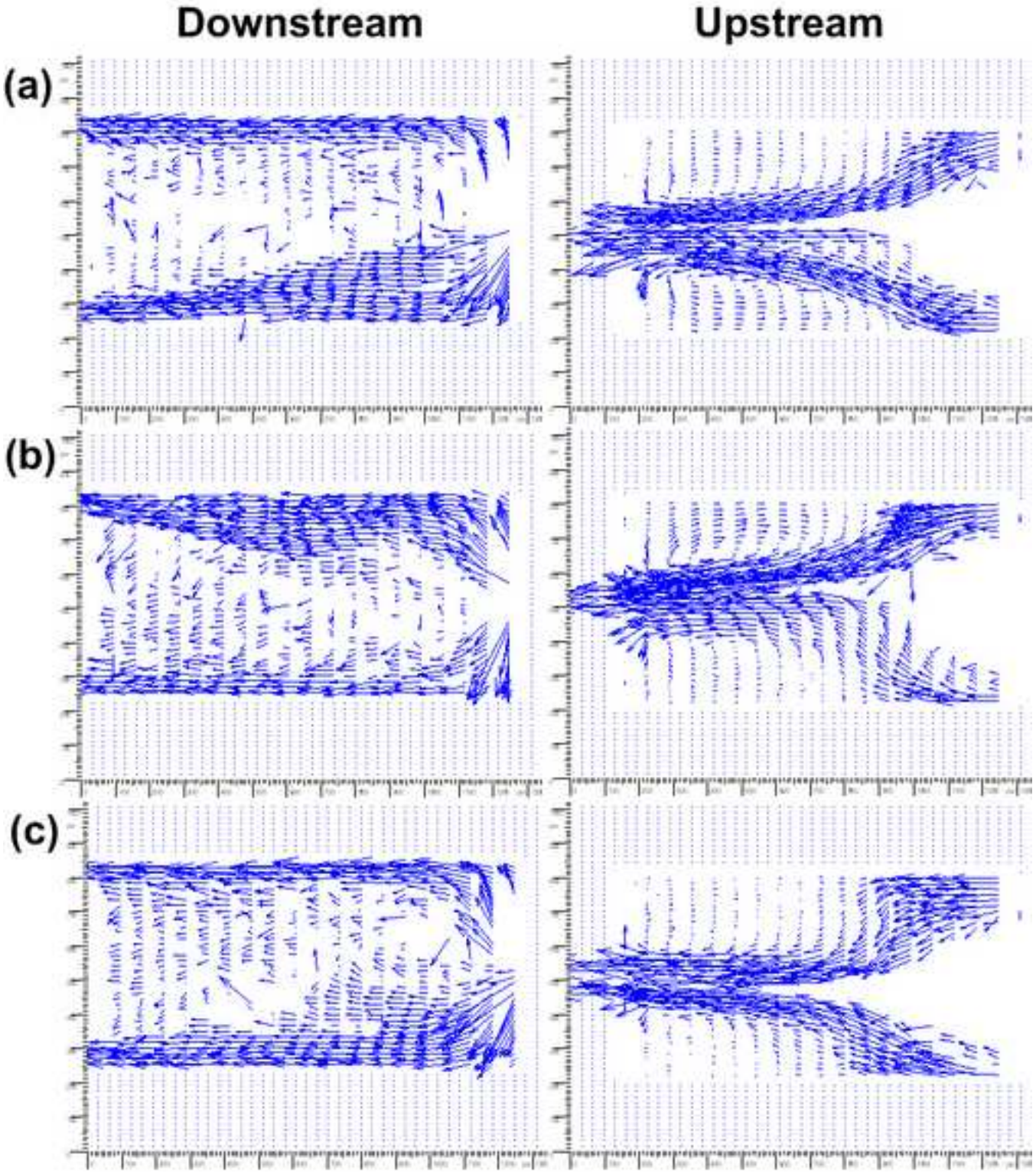

Figure5

Click here to download high resolution image

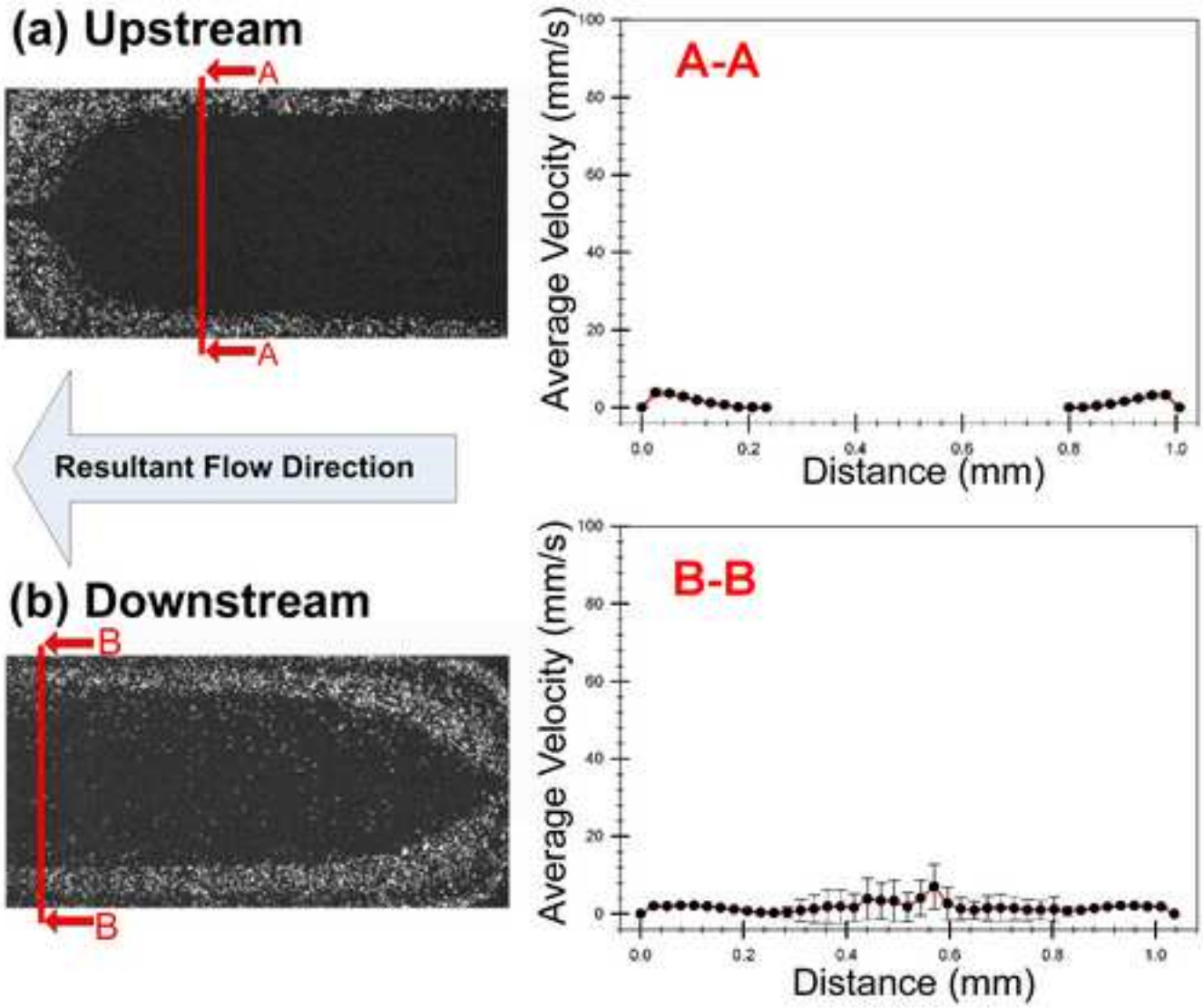

Figure6

Click here to download high resolution image

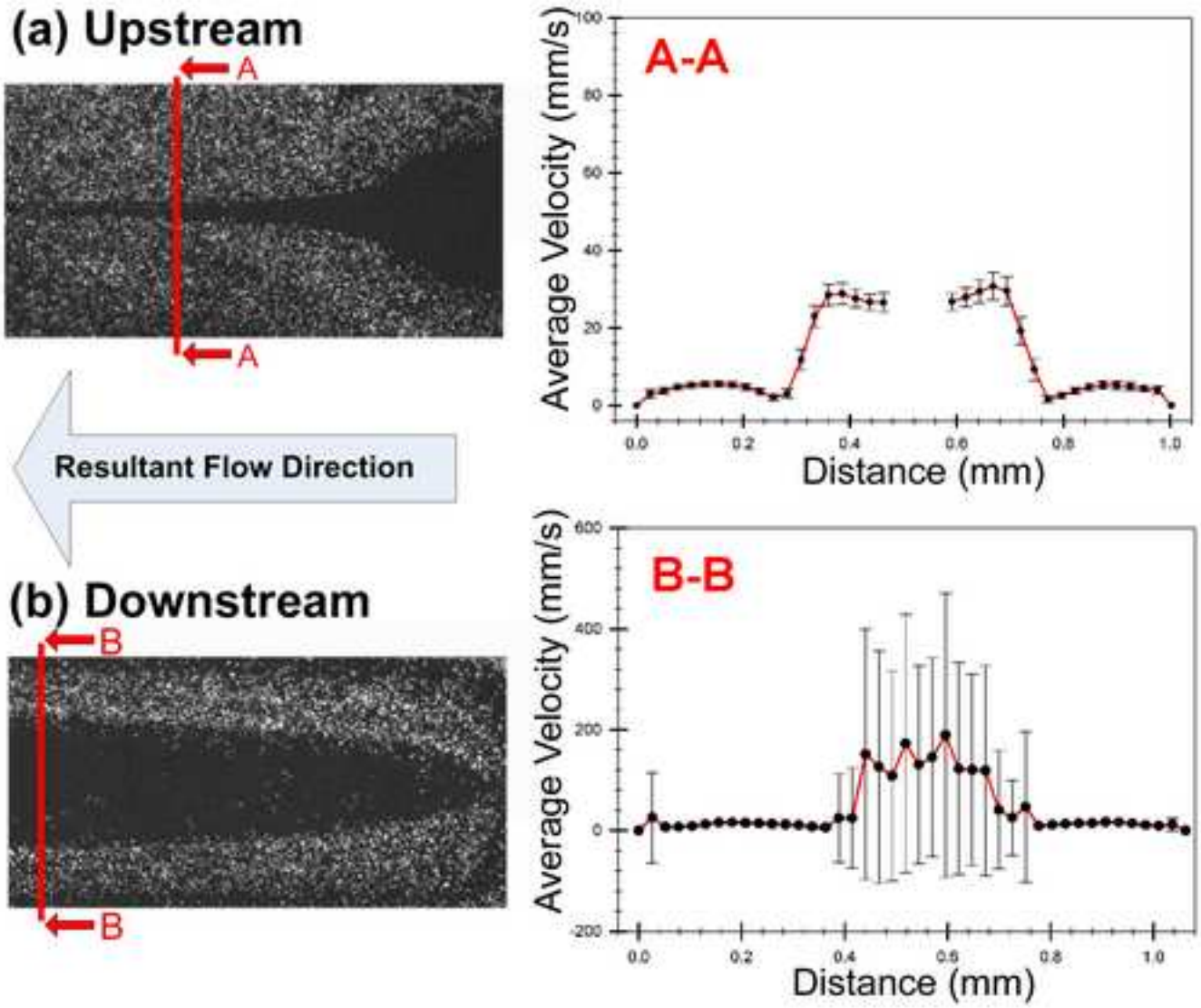

Figure7

Click here to download high resolution image

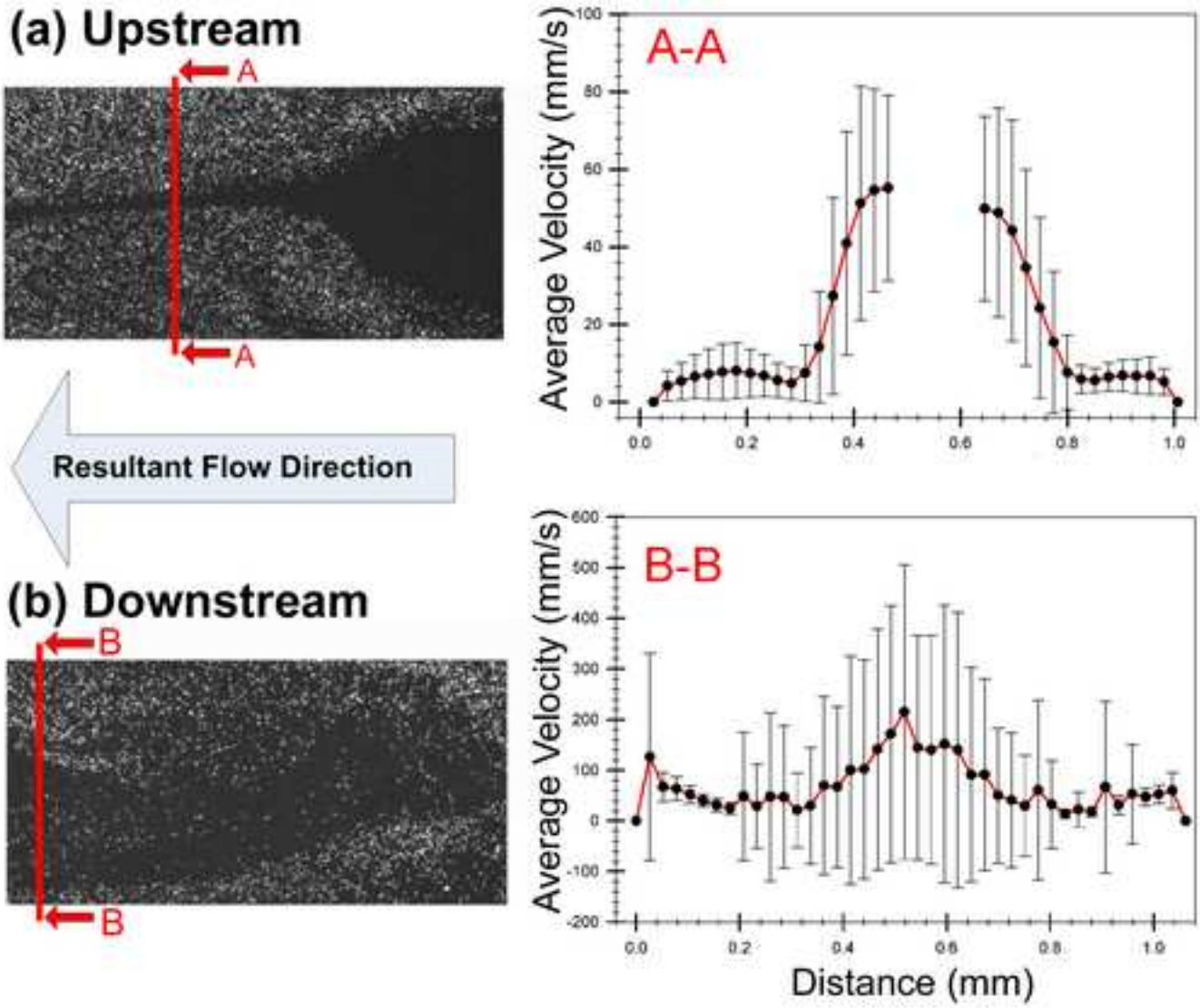

Figure8
Click here to download high resolution image

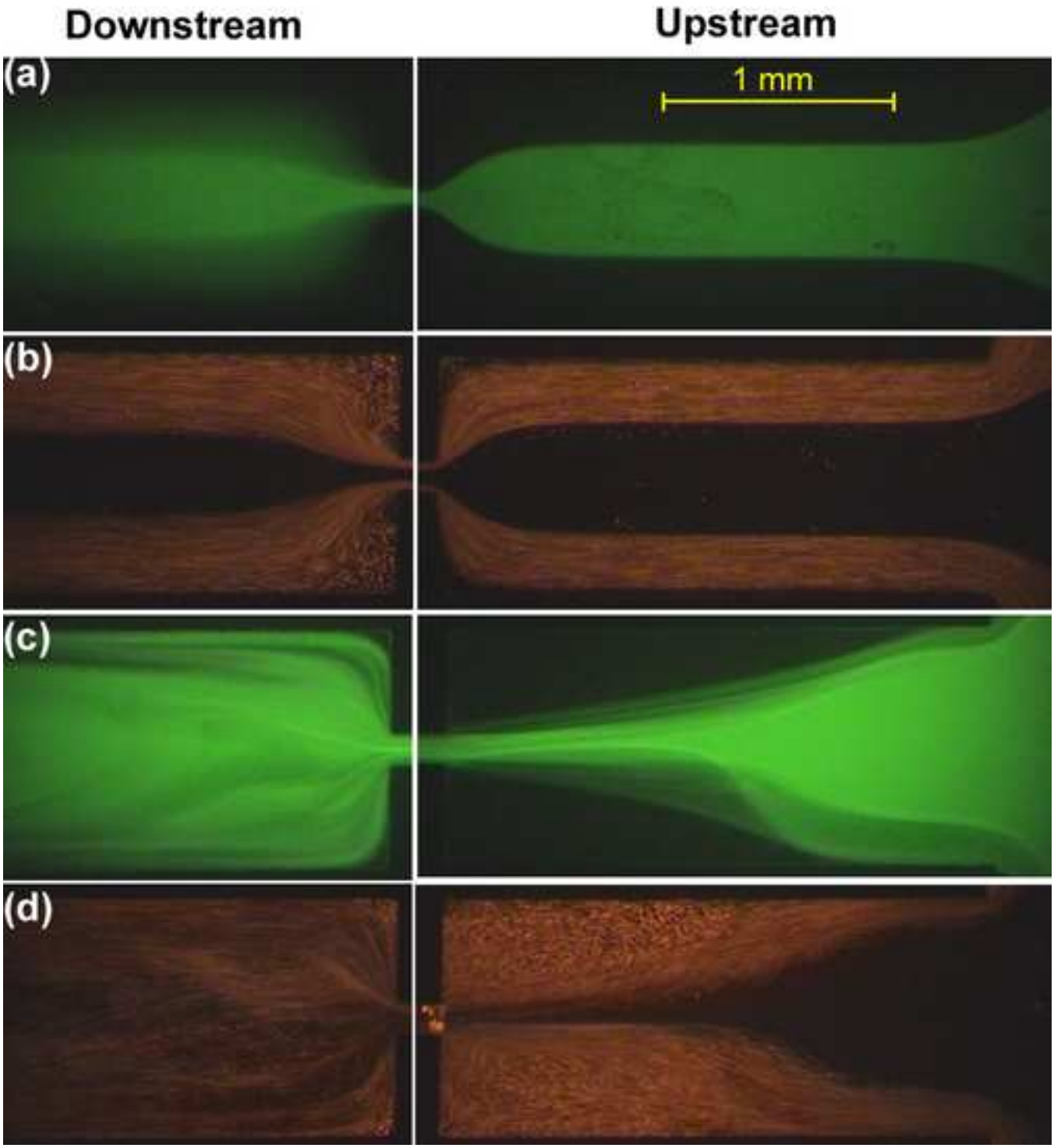

Figure9
Click here to download high resolution image